2024-10-11

Launaea cornuta (wild lettuce) leaf extract: phytochemical analysis and synthesis of silver-zinc oxide nanocomposite

Makauki, Elizabeth

IOP Science

https://doi.org/10.1088/2632-959X/ad80b1

PAPER • **OPEN ACCESS**

Launaea cornuta (wild lettuce) leaf extract: phytochemical analysis and synthesis of silver-zinc oxide nanocomposite

To cite this article: Elizabeth Makauki *et al* 2024 *Nano Ex.* **5** 045003

NANO EXPRESS

PAPER

Launaea cornuta (wild lettuce) leaf extract: phytochemical analysis and synthesis of silver-zinc oxide nanocomposite

Elizabeth Makauki[1], **Mwemezi Rwiza**[1], **Revocatus Machunda**[1] **and Onita D Basu**[2]

[1] School of Materials Energy Water and Environmental Sciences, Nelson Mandela African Institution of Science and Technology, Arusha, Tanzania

[2] Department of Civil & Environmental Engineering, Faculty of Engineering & Design, Carleton University, Ottawa, Canada

E-mail: elizabeth.makauki@nm-aist.ac.tz

Keywords: microbial inhibition, phenolic content, green synthesis, reactive oxygen species (ROS)

Supplementary material for this article is available online

OPEN ACCESS

RECEIVED
10 June 2024

REVISED
10 August 2024

ACCEPTED FOR PUBLICATION
27 September 2024

PUBLISHED
11 October 2024

Abstract

Access to quality drinking water is an essential human right and a fundamental aspect of human dignity, yet a challenge to many in developing countries. Over 2 billion people worldwide lack access to quality drinking water due to microbial contamination, among other factors. Silver-doped zinc oxide impregnated activated carbon nanocomposites, Ag-ZnO-AC NCs, a strong antimicrobial agent have been used at point-of-use to treat water treatment. Green synthesis of Ag-ZnO-AC NCs has played a vital role since it leads to the acquisition of non-toxic nanocomposites compared to chemical synthesis. In this study, Ag-ZnO-AC NCs were green-synthesized using *Launaea cornuta* leaf extract as a source of reducing and capping agents in place of synthetic chemicals. Antioxidants from *Launaea cornuta* (Wild Lettuce) leaves were extracted using 0, 50, and 100% EtOH solvents with different volumes and extraction circles. The highest phenolic (11044 ± 63 μg) and antioxidant (44112 ± 894 μg) contents were extracted using 50% EtOH and 20 ml of extract solvent with $p < 0.05$. The SEM and TEM images of the synthesized Ag-ZnO-AC NCs show the formation of highly porous AC with sheet-like structures and successful Ag-ZnO NCs impregnation within the pores and on the surface of the AC. Based on the inhibition zone, the antimicrobial activity of the Ag-ZnO AC NCs had significant results with 14.00 ± 0.37 for *E. coli* and 17.33 ± 0.36 mm for *S. aureus*, $p < 0.05$. These results confirm the significance of *Launaea cornuta* (Wild Lettuce) as a source of antioxidants that can be used as reducing and capping agents to synthesize Ag-ZnO-AC NCs.

Introduction

Access to quality drinking water is an essential human right and a fundamental aspect of human dignity as acknowledged by Sustainable Development Goal 6 [1]. Despite its importance more than 2 billion people worldwide lack access to quality drinking water [2]. Microbial contamination is one of the causes of water quality deterioration worldwide and is the largest cause of waterborne diseases and deaths [3]. For instance, amoeba, typhoid and cholera are waterborne diseases reported to be associated with consumption of contaminated drinking water causing approximately 485,000 deaths per annum [4].

Water quality is related to natural and anthropogenic factors such as water-rock interactions, hydrology, land cover, land use, climate and human operational factors [5–8]. To ensure access to quality water it is necessary to monitor the quality of water from the sources to the consumer level. Point-of-use water treatment (POUWT) systems such as membrane and ceramic water filters are alternatives to quality drinking water access at the consumer level [9, 10]. POUWT systems are packed with antimicrobial agents like zinc oxide (ZnO) to achieve microbial disinfection during water treatment [11, 12].

ZnO is a non-toxic, eco-friendly semiconductor widely used as an antimicrobial material due to its wide band gap (3.36 eV) and high exciton binding energy (60 meV) [13, 14]. In the presence of sunlight or UV ZnO

produces positive holes (h+) and electrons (e-) referred to as electron–hole pairs which are responsible for the generation of reactive oxygen species (ROS). The ROS can introduce oxidative stress in bacteria cells leading to their death [15]. The electron–hole pairs of ZnO have a rapid recombination rate as they favour light absorption in the UV over the visible region, leaving the visible light unutilised [16]. Doping of silver (Ag) in the ZnO lattice has promoted the use of light in the visible region and prolonged the recombination time of the electron–hole pairs [17]. Asamoah *et al* doped Ag into ZnO resulting in the reduction of the energy band gap from 3.37 to 2.88 eV. The doped ZnO improved its ROS generation and antimicrobial activity [18, 19]. Doping of Ag into ZnO brings about a stronger electron storage capacity because as a semiconductor ZnO can easily inherit electrons to Ag-NPs therefore sustainable formation of ROS [20, 21].

Despite, the improved antimicrobial efficiency of silver-doped zinc oxide nanocomposites (Ag-ZnO NCs) in water treatment its use should consider the exposure limit to prevent any effect brought by excess uptake [22]. For such reasons, Ag-ZnO NCs have been impregnated into porous materials such as activated carbon (AC) and graphene [23–26]. Activated carbon introduces a controlled release of metallic ions, allowing for a predictable, stable, and sustainable water treatment process [13, 27]. It enhances the efficiency of water purification by a synergetic combination of the AC adsorption and the Ag-ZnO NCs antimicrobial activity [27, 28].

Studies have documented the synthesis of silver zinc oxide nanocomposites impregnated activated carbon (Ag-ZnO-AC NCs) using chemical methods with promising antimicrobial activities [27, 29]. Chemical synthesis uses toxic and carcinogenic chemicals that produce contaminated nanocomposites not fit for human consumption [30, 31] To the best of our knowledge, there is limited research and report on the green synthesis of Ag-ZnO-AC NCs. Green synthesis brings about toxic-free and cleaner composites that can be trusted in uses related to human consumption such as water treatment. Plant extracts especially from medicinal plants have been used in green synthesis since they are good sources of secondary metabolites [32–35]. The metabolites such as flavonoids, alkaloids, tannins, proteins, polyphenols, terpenoids, and saponins act as hydrolyzing/reducing agents and capping agents in the synthesis of nanoparticles in place of synthetic chemicals [36–39].

This research explores the novel potential of *Launaea cornuta* (Wild Lettuce) leaf extract in green synthesis of Ag-ZnO-AC NCs from nitrates of Ag and Zinc. The antimicrobial efficiency of the synthesized Ag-ZnO-AC NCs was tested against gram-positive (*Staphylococcus aureus*) and gram-negative (*Escherichia coli*) bacteria through a well-diffusion method. Furthermore, the study explores the effectiveness of solvent type in the total phenollic and antioxidant contents extraction of secondary metabolites.

Materials and methods

Materials

Analytical quality $AgNO_3$ (99.99%), $Zn(NO_3)_2$ (99.99%), NaOH (98%), Ethanol (99.5%), KOH (98%), Folin, Na_2CO_3 (99.5%), Gallic acid(97.5%), ABTS solution, and Trolox (97%) were purchased from Aldi-rich and used without modification. Water hyacinth was collected from Lake Victoria, Mwanza Tanzania. *Launaea cornuta* leaves were harvested from the fields of the Nelson Mandela African Institution of Science and Technology, Nambala village, Arusha region, Tanzania, at coordinates 3°23′58″S 36°47′48″E. The plant was properly identified and stored at the National Herbarium of Tanzania (NHT) under the Tanzania Plant Health and Pesticides Authority (TPHPA) with the reference number KA51/2023 [40]. All procedures for collecting plant materials followed the relevant institutional, national, and international regulations and guidelines.

Methods

Launaea cornuta leaf extract preparation

Launaea cornuta leaves were thoroughly washed using tap water followed by double distilled water three times. The leaves were then dried using a freeze drier for 48 h before grounding using an electric mortar to a fine powder. *Launaea cornuta* leaf extract was obtained using ultrasound-assisted solid–liquid extraction (USAE). 0.5 g of the fine powder was added into a 50 ml Eppendorf tube followed by 5 ml of milli-aqua water. The mixture was hand mixed gently for a minute before immersing in an ultrasonic bath (frequency 35 kHz; power 60–120 W; Sonorex TK 52; Bandelin electronic, Berlin, Germany) for 10 min at 30 °C. The samples were centrifuged at 7830 rpm for 5 min and the supernatant was collected with a Pasteur pipette and filtered using No. 1 Whatman filter paper using a vacuum filter.

The extraction was repeated using different conditions to create the optimum extraction conditions. The extract volumes were varied by 5, 10 and 20 ml for each extraction solvent used. Extraction solvents based on the water-ethanol ratio were used to vary the polarity of the solvent. In this case, 100% water (0%EtOH), 50% water (50%EtOH) and 100% ethanol (100%EtOH) were used as solvents. The extraction cycles used were 2, 3, or 4 for a sample. The extraction process was done in triplicates, n = 3, to allow reproducibility.

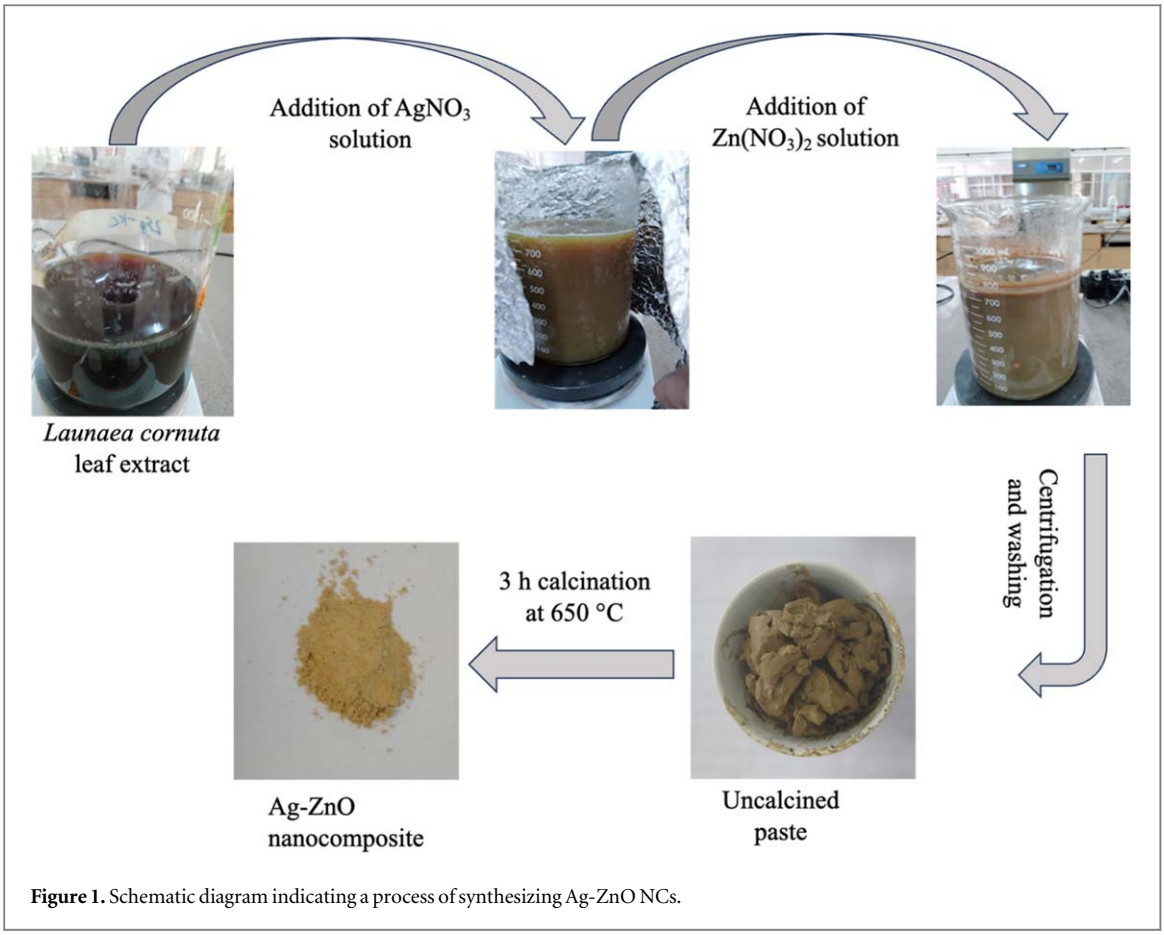

Figure 1. Schematic diagram indicating a process of synthesizing Ag-ZnO NCs.

The alcoholic supernatants were evaporated to dryness using a rotary evaporator while the water supernatants were dried using a freeze drier. The mass of each dried sample was recorded. Milli aqua water was used to dilute the dry samples into a common concentration of 10 mg mL^{-1}. It was also used to calculate the total phenolic and antioxidant contents extracted from the dry samples of *Launaea cornuta*. The solutions were centrifuged to remove suspended solids before storing them at 4 °C ready for phytochemical analysis.

Total phenolic content analysis

The total phenolic content of the *Launaea cornuta* leaf extracts was determined by the Folin-Ciocalteu reagent method [41]. In this analysis, 400 μl of milli aqua water was added into a 1 ml cuvette followed by 80 μl *Launaea cornuta* leaf extracts, 40 μl folin, and lastly 480 μl 10.75% Na_2CO_3. The resulting mixture was incubated at room temperature for 30 min before absorbance reading by a mass spectrometer at 765 nm. Gallic acid was used as standard while water was used as blank in this experiment. All the tests were performed in triplicates to ensure accuracy (n = 9). Total phenolic content was determined from the standard curve equation and expressed as gallic acid equivalent (GAE) expressed in mg of extracted compound over g of dry leaf sample.

Total antioxidant content analysis

The free radical scavenging activity (antioxidant activity) of *Launaea cornuta* leaf extracts (DPPH) was determined as described by Guzzetti *et al* [42]. 50 μl of 1 mg ml^{-1} *Launaea cornuta* leaf extracts was added into a 1 ml cuvette followed by 950 μl ABTS. The sample was well mixed and incubated for 6 min before reading the absorbance using a spectrophotometer at 734 nm wavelength. Water was used as blank while Trolox was used as a standard solution in this experiment. The total antioxidant content is expressed as mg TE (Trolox Equivalent) per gram of leaves and $ABTS^{+}$ inhibition percentage.

Synthesis of Ag-ZnO NCs

Synthesis of Ag-ZnO NCs was adopted from Makauki *et al* using optimum conditions reported in that study [40]. As presented in figure 1, in a 250 mm conical flask, 92 ml of *Launaea cornuta* leaf extract was added and introduced to stirring on a hot plate. 8 ml of 0.1 M $AgNO_3$ was added dropwise to the leaf extract under vigorous stirring to allow maximum ionic interaction. The reaction proceeded for 15 min before adding 2.97 g of $Zn(NO_3)_2$ at pH 7. The reaction ran for 2 h at a 70 °C temperature. The resulting mixture was centrifuged at

4000 rpm for 10 min to extract the nanocomposite paste. The solid residue was collected and washed twice using 50% ethanol followed by drying at 100 °C for 24 h. The dry sample was calcined at 650 °C for 3 h using a box furnace.

Synthesis of AC

AC was synthesized from water hyacinth following a route reported by Makauki *et al* with some modifications [43]. Water hyacinth was collected from Lake Victoria, and washed thoroughly with tap water after removing the roots. The plant material was washed with distilled water and dried in a shed for 2 weeks. The dried precursor was fragmented into small pieces and powdered using an electric grinder. 5 g of the powdered precursor was carbonized in a carbolite horizontal tubular furnace (CTF 12/65/550) under N_2 inert atmosphere at 650, 750, and 850 °C for 1 h with a heating ramp rate of 10 °C per min. The carbon obtained was activated using KOH in a 1:1 mass ratio at 700 °C for 30 min in the carbolite tubular furnace under N_2 inert atmosphere. The resulting activated carbon was washed using distilled water to a pH of 7. The AC was then dried at 100 °C in an oven for 12 h. The dry samples were stored in tight dry containers ready for the impregnation with Ag-ZnO NCs.

Impregnation of Ag-ZnO NCs into AC

Ag-ZnO-AC NCs were prepared by mixing 1 g of Ag-ZnO NCs and 1 g of AC in 10 ml of milli aqua water. The mixture was vigorously stirred for 1 h followed by prob sonication for another 1 h. The sample was then dried and kept tight for characterization and antimicrobial testing. The prepared samples were named C-T, AC-T, and Ag-ZnO-AC-T where C, AC, Ag-ZnO-AC, and T stand for carbon, activated carbon, silver zinc oxide impregnated activated carbon, and carbonization temperature respectively.

Characterization

The leaf extract functional groups were identified using attenuated total reflection-Fourier transform infrared (ATR-FTIR) spectroscopy (Bruker Optic GmbH 2011, alpha model, Laser class 1). The crystalline nature of synthesized nanomaterials was analyzed at Carleton University using Rigaku XtaLAB Mini II Single-Crystal x-ray Diffractometer (427 SC) equipped with analyzer scanning mode of CuKα wavelength (λ) = 1.540598 Å, 45 kV-30 mA and $2\theta/\theta$ with the spectrum range between 10 and 90 degrees and 0.026 scan step size. The morphologies of the synthesized nanocomposites were characterized by Field emission scanning electron microscopy (FE-SEM)-EDS using Tescan Vega-II XMU Scanning Electron Microscope. The cross-sectional morphology (TEM) of the nanocomposites and Selected area elemental diffraction (SAED) was determined by high-resolution transmission electron microscopy—HR-TEM (FEI Tecnai G2 F20 Transmission Electron Microscope).

Microbial assay of the synthesized nanocomposites

The antimicrobial solution was prepared by adding 10, 17, and 34 mg of Ag-ZnO-AC NCs to 20, 34, and 68 µl of milli aqua water. The mixture was vortexed for 2 min for proper mixing. Gram-negative (*Escherichia coli*-ATCC 25922) and gram-positive (*Staphylococcus aureus*- ATCC 25923) bacterial strains with a spectrophotometric absorbance of 0.1 ± 0.01 were used to assess the antimicrobial efficacy through well diffusion method [44]. Sterilised nutrient agar media was prepared by mixing 5.0 g peptone, 5.0 g NaCl, 1.5 g beef extract, 1.5 g yeast extract, and 15.0 g agar in 1 L milli aqua water. The mixture was autoclaved at 100 °C for 20 min. After cooling, 50 ml of the nutrient agar was poured into an agar plate followed by 1 ml of 0.1 ± 0.01 desired bacteria strain, the two were well mixed. After solidification, 3 holes of 6 mm width were formed in the agar using the back of a pipette tip and the prepared nanocomposite mixture was added into the holes using pipette. The inoculated discs were then incubated for 24 h at 37 °C and the zone of inhibition (ZOI) was measured in millimetres of diameter. Agar plates with bacteria only (without Ag-ZnO-AC NCs) were used as positive control while agar plates with nanocomposites only (without bacteria) were used as negative control.

Results and discussion

Total phenolic content and antioxidant analysis

The calibration curve of the isolated gallic acid was established using a spectrophotometer at 765 nm. The calibration curve equation was $y = 0.0078x-0.035$ and $R^2 = 0.9991$ as illustrated in the supplementary information S1. The total phenolic content of *Launaea cornuta* leaf extracts was expressed as gallic acid equivalent µg(GAE)/g of solid sample from the established gallic acid standard curve. Figure 2(a) and table 1 demonstrate the effect of extraction volume and cycles on the amount of phenolic content. As the extraction volume and cycles increase the total phenolic content extraction from *Launaea cornuta* leaves also increases with significance, $p < 0.05$. When 5, 10, and 20 ml of extraction solvent were used, the higher total phenolic content

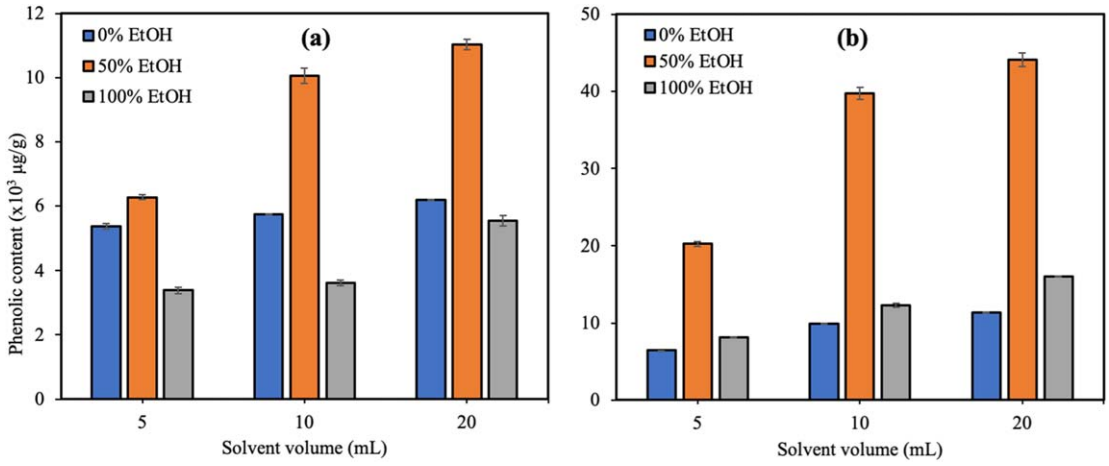

Figure 2. Total phenolic (a) and antioxidant contents (b) of *Launaea cornuta* leaf extract.

Table 1. Percentage of total phenolic and antioxidant content of *Launaea cornuta* leaf extract.

% EtOH	Solvent volume (ml)	Phenolic content (%/g)	Antioxidants content (%/g)
0	5	1.072 ± 0.014	1.281 ± 0.004
0	10	1.133 ± 0.004	1.954 ± 0.018
0	20	1.223 ± 0.007	2.237 ± 0.007
50	5	1.223 ± 0.014	3.952 ± 0.058
50	10	1.921 ± 0.049	7.621 ± 0.193
50	20	2.152 ± 0.032	8.598 ± 0.173
100	5	0.662 ± 0.020	1.599 ± 0.005
100	10	0.704 ± 0.016	2.392 ± 0.052
100	20	1.080 ± 0.033	3.127 ± 0.016

was obtained with 20 ml of solvent ($p < 0.05$). High phenolic content was also observed with 4 extraction circles compared to 2 and 3 cycles as indicated in figure 3. Extraction solvent plays a vital role in optimal extraction since it involves polarity. In this regard 100%, 50%, and 0% EtOH were used as extraction solvents. Total phenolic contents were maximumly extracted using 50% EtOH solvent with the order of 50% EtOH > 0% EtOH > 100% EtOH, $p < 0.05$, as reported elsewhere [41]. Water and ethanol have different polarities which might have influenced the solubility of the antioxidants present in *Launaea cornuta* leaves when used together. The optimal extractions were 50% EtOH, 20 ml solvent, and three extraction cycles with the total phenolic content reaching 11044.33 ± 62.51 µg GAE/g also illustrated in the supplementary information S3.

The antioxidant scavenging activity of *Launaea cornuta* leaf extract in different conditions was determined using $ABTS^+$ with the calibration curve equation y = 0.0013x-0.0069 and $R^2 = 0.9996$ as illustrated in the supplementary information S2. The $ABTS^+$ inhibitory activity (%) of the extract samples followed the order 50% EtOH > 0% EtOH > 100% EtOH as illustrated in table 1. An increase in extraction cycles and volume increased the $ABTS^+$ inhibiting effect of the samples, figure 2(b). The highest inhibition was observed when 20 ml of 50% EtOH was used in three extraction cycles in which the inhibition was 8.598 ± 0.173% (44174 ± 94 µg TE per gram) also illustrated in the supplementary information S4. The results had a significant *p*-value of less than 0.05 for all conditions showcasing its significance. The higher liquid-to-solids ratio increases the dissolution of the metabolites to the solvent and faster extraction rates [45].

ART-FTIR studies

Attenuated total reflection-Fourier transform infrared (ATR-FTIR) studies confirmed the presence of secondary metabolites in *Launeae cornuta* leaf extract as indicated in figure 4. Flavonoids, alkaloids tannins, and saponins are confirmed to be present in the leaf extract. The 1315 cm^{-1} band indicates C-C starching and the 3292 cm^{-1} broad strong band is O-H and N-H stretching vibration indicating the presence of flavonoids and tannins [46–48]. The 635 cm^{-1} band represent the N-H stretching. The 1006 cm^{-1} bands represent the C-N stretching of the aliphatic amines. The 1315 cm^{-1} band represent the C-N stretching of the aromatic amines [49]. The N-H

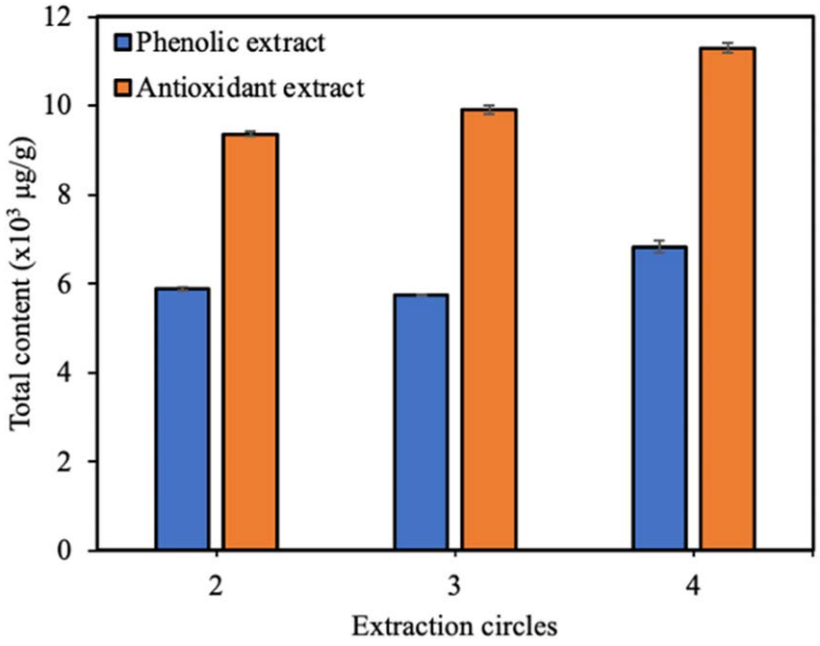

Figure 3. Effect of the extraction cycle on total phenolic and antioxidant contents of *Launaea cornuta* leaf extract.

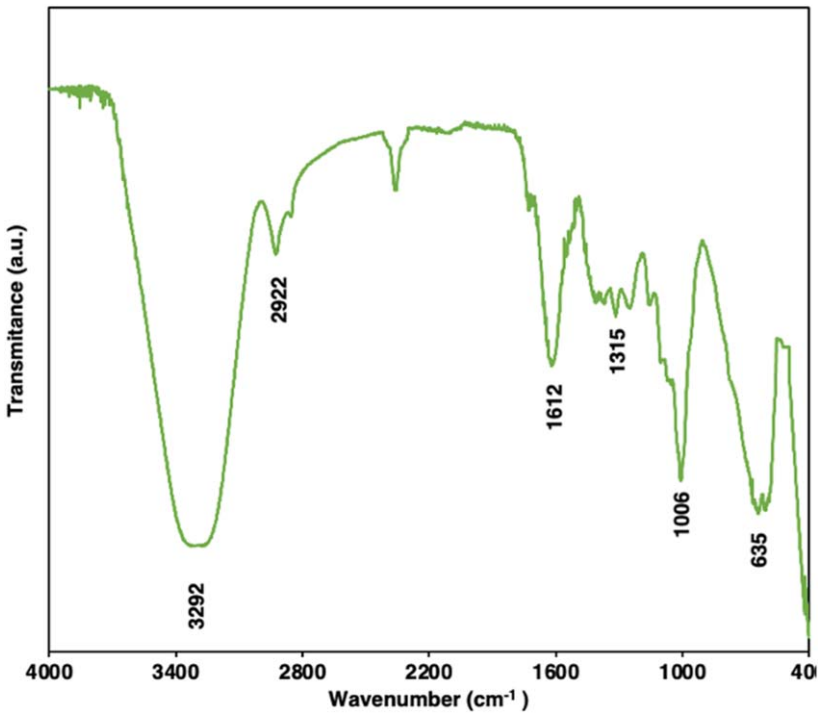

Figure 4. FTIR patterns of *Launaea cornuta* leaf extract.

and C-N stretching vibrations confirm the presence of alkaloids in the leaf extract [50]. Saponins are presented by C-H and C=C stretching vibrations which are verified by the presence of 2922 and 1612 cm^{-1} bands. Alkaloids have reducing power they reduce the metallic ions to metallic atoms leading to the formation of the nanoparticles. The flavonoids, saponins, and tannins are natural surfactants. They regulate the size of the nanoparticles and prevent agglomeration through steric hindrance around the nanoparticles [51].

X-ray diffraction (XRD)

The crystalline nature and particle size of synthesized nanomaterials were analysed using x-ray diffraction (XRD). The XRD pattern of C-850 indicates the presence of peaks at 29.87 and 40.51; AC-850 shows peaks at 29.

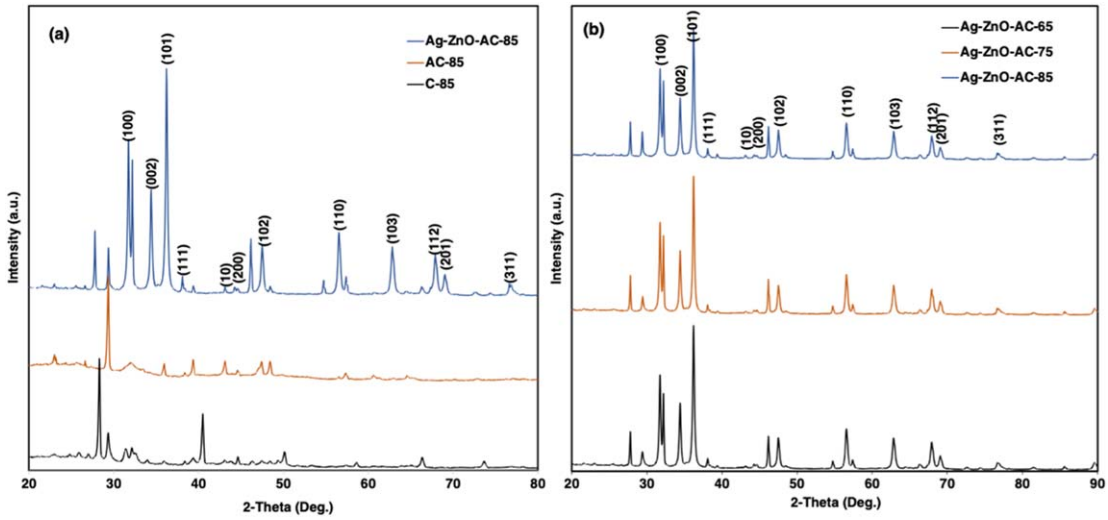

Figure 5. XRD patterns of (a) carbon, activated carbon, and impregnated activated carbon (b) impregnated activated carbon at different carbonation temperatures.

34 and 43.15. The two peaks in C-850 and AC-850 correspond to the planes 002 and 10 of graphitic carbon diffraction according to diffraction card JCPDS no. 75–1621 [52]. The peaks displayed around 23 degrees explain the random aromatic carbon sheets confirming the formation of sheet-structured carbon [53]. As illustrated in figure 5(a), More peaks are observed in the carbon matrix indicating the presence of macro- and micro-elements such as manganese, calcium, and silicon present in the plant matrix as reported elsewhere and proved by the EDS graphs of the same sample [54, 55]. The peak displayed at 28.3 degrees corresponds to SiO_2 [56]. The depicted pattern of Ag-ZnO-AC-850 in figure 5(a) is for Ag-ZnO AC NCs. It reveals four prominent peaks at 2θ values around 38.10, 44.28, and 77.38 degrees, corresponding to the crystal planes of (111), (200), and (311) [57]. These peaks affirm the face-centred-cubic (fcc) crystalline nature of the AgNPs, with lattice parameters a = b = c = 4.088 Å, as evidenced by a comparison with the silver standard powder diffraction card, JCPDS, file No. 04–0783 [58, 59]. Diffraction peaks at 2θ values 31.74, 34.38, 36.18, 47.42, 56.48, 62.80, 67.84, and 68.24 degrees, correspond to the crystal planes (100), (002), (101), (102), (110), (103), (112), and (201) of ZnO marching the ZnO standard powder diffraction card JCPDS, card no. 36–1451, affirming the presence of ZnO NPs in the nanocomposite matrix [60]. This pattern suggests the typical hexagonal wurtzite structure ZnO in space group P 63 mc as reported elsewhere [40]. These results confirm the successful impregnation of Ag-ZnO in the activated carbon matrix. Figure 5(b) indicates XRD patterns of the Ag-ZnO-AC at different carbonation temperatures. There is no significant shift of the peaks in the sample patterns since the same Ag-ZnO was impregnated in the AC matrix. All the samples indicated the presence of Ag-ZnO NPs.

The average particle of the synthesized Ag-ZnO-AC samples was calculated using the Debye–Scherrer equation below where, K is the Scherrer constant (0.94), λ is the specific wavelength of the x-ray used which is 0.154 nm, β is the full width at half maxima, θ is the diffraction Bragg angle and D is the average crystallite size in nm.

$$D = \frac{K\lambda}{\beta_{2\theta} \cos\theta} \tag{1}$$

The average particle size for Ag-ZnO-AC-650, I Ag-ZnO-AC-750 and Ag-ZnO-AC-850 was 50.87, 44.35 and 40.22 nm respectively. The particle sizes show Ag-ZnO NCs domination as observed in the patterns in figure 5(b). The crystalline size of the Ag-ZnO-AC NCs displayed an increase compared to the size of the same material [40]. This is believed to be caused by the intra-granular coupling between the metallic composite and the activated carbon [27]. The XRD patterns of the AC-650, AC-750, AC-850, C-750 and C-850 indicated smaller particle size compared to the Ag-ZnO-AC as a result of the existence of the microelements present in the water hyacinth plant matrix [54].

Field emission scanning electron microscopy (FE-SEM)

The FE-SEM images of water hyacinth AC project complex irregular sheet-like morphologies as presented in figure 6. The complexity might be contributed by the aggregation of mineral compounds in the plant matrix [61]. Figures 6(a)–(c) show the effect of carbonation temperature on the particle size of the carbon materials. The fragmentation on the C increases as the temperature from 650 to 850 °C. An increase in carbonation

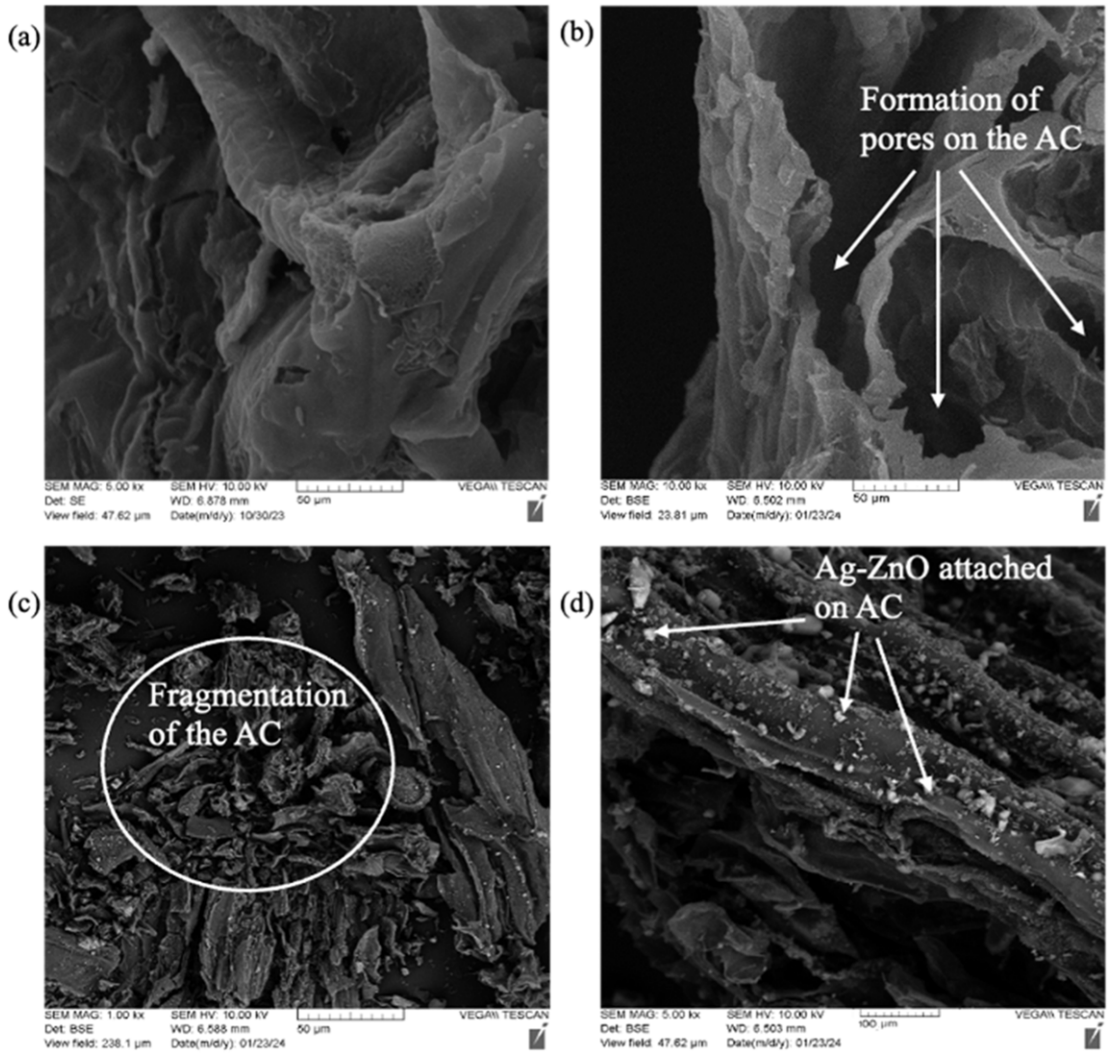

Figure 6. SEM images of (a) C-650 (b) C-750 (c) C-850 (d) Ag-ZnO-AC-650.

temperature increases the rate of organic matter dehydration, decomposition, and volatilization from the plant biomass therefore, there is a widening of the biochar micropores [54]. These pores provide more surface area for the attachment of the Ag-ZnO NCs. Figure 6(d) indicates almost a uniform distribution of the Ag-ZnO NCs in the activated carbon matrix represented by the brighter particles. Activated carbon not only supported the attachment of the NCs but also provided controlled release of the NCs and adsorption during the matrix application.

The selected area electron diffraction (SAED) pattern of the Ag-ZnO-AC in supplementary information S5(a-b) indicates the presence of both Ag and ZnO as elaborated by d-spacing values. The d-spacing 2.347A corresponds to the crystal planes of (111) which confirms the face-centred-cubic (fcc) crystalline nature of the AgNPs [59]. The d-spacing 2.82A corresponds to the crystal planes 100 of ZnO confirming the presence of ZnO NPs in the nanocomposite matrix [60]. Figures 7(a)–(e) is the selected area electron mapping which indicates the presence of Ag, Zn, O, and C. EDS spectra figure 7(f) provides more evidence as it shows the presence and distribution of Ag, Zn, O, and C in the activated carbon matrix evidencing a successful impregnation of Ag-ZnO in the AC. AC controls the Ag-ZnO agglomeration by improving the nanoparticles distribution on its surface.

High-resolution transmission electron microscopy (HR-TEM)

Figure 8 represents the TEM images of AC and Ag-ZnO-AC. The TEM image of the un-impregnated AC figure 8(a) displays sheetlike structures corresponding to the results presented in XRD and SEM images. Figure 8(b) represents Ag-ZnO-AC indicating an introduction of spherical nanoparticles in the AC sheets. These spherical structures represent the Ag-ZnO NCs impregnated in the AC matrix. The size of these nanoparticles as determined by the TEM machine is between 16–21 nm [40]. It can be seen clearly that the Ag-ZnO NCs are integrated into the AC sheets suggesting the controlled integration between AC and Ag-ZnO. The Ag-ZnO NCs

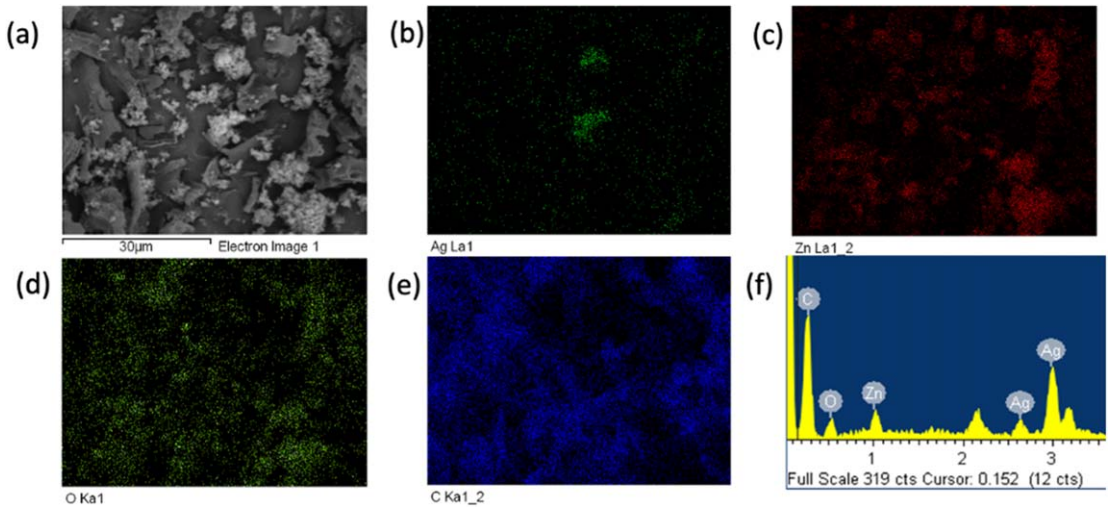

Figure 7. (a) Electron mapping of Ag-ZnO-AC-850 showing the presence of (b) Ag, (c) Zn, (d) O and (e) carbon. (f) Represents the energy-dispersive x-ray spectroscopy (EDS) pattern of Ag-ZnO-AC-850.

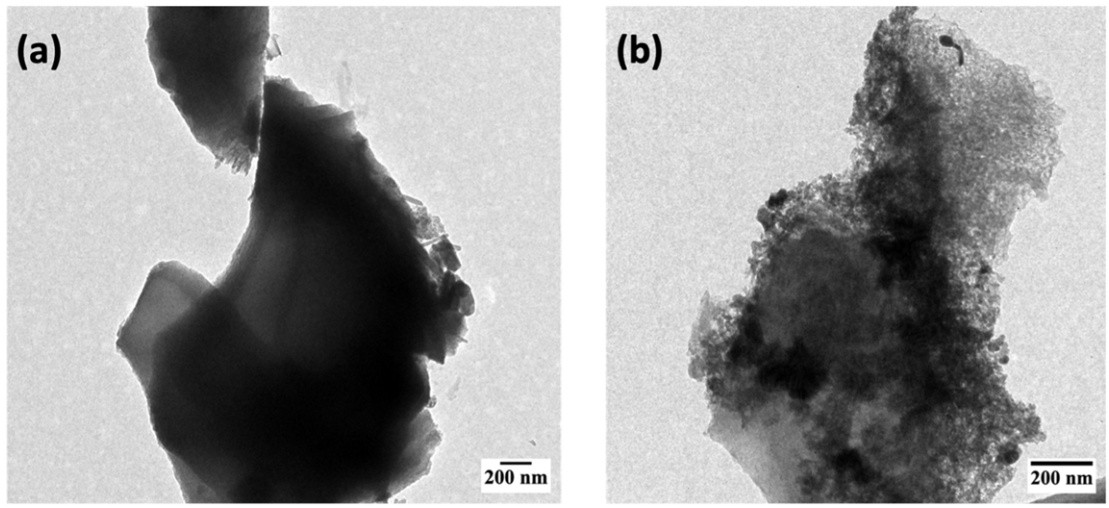

Figure 8. TEM images of (a) AC-850 and (b) Ag-ZnO-AC-850.

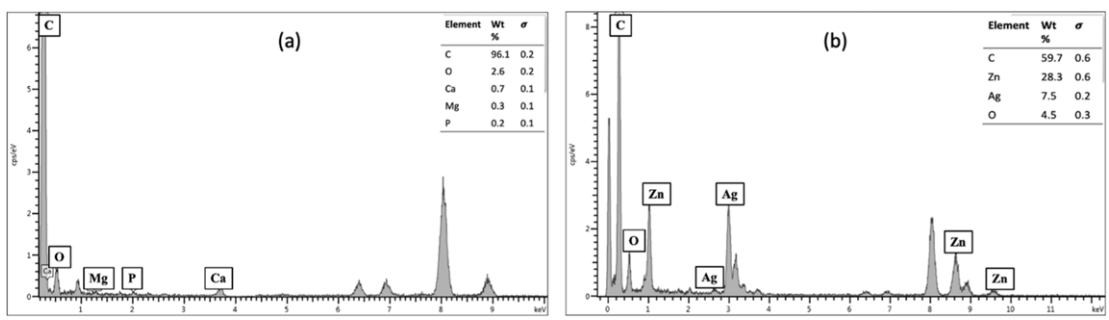

Figure 9. Energy-dispersive x-ray spectroscopy (EDS) pattern of the (a) AC-850 and (b) Ag-ZnO-AC-850.

occupied the carbon pores created during activation. The TEM-EDX in figure 9(a) indicates the presence of C as the main component (50.8%) followed by O, K, P, Mg, and Si in order of decreased occurrence. There was also a trace occurrence of Cl. These elements are part of the plant matrix as reported by Masto *et al* in biochar prepared

Table 2. The microbial inhibition of the synthesized Ag-ZnO AC NCs on *E. coli* and *S. aureus*.

Sample Mass (mg)	*E. coli* ZOI (mm)			*S. aureus* ZOI (mm)		
	10	17	34	10	17	34
Ag-ZnO-AC-65	11.50 ± 0.22	12.33 ± 0.17	13.33 ± 0.21	13.83 ± 0.31	15.50 ± 0.22	16.17 ± 0.31
Ag-ZnO-AC -75	11.92 ± 0.27	12.50 ± 0.22	13.67 ± 0.33	14.17 ± 0.31	16.00 ± 0.26	16.50 ± 0.43
Ag-ZnO-AC -85	12.17 ± 0.21	12.83 ± 0.17	14.00 ± 0.37	14.83 ± 0.31	16.00 ± 0.26	17.33 ± 0.36

Table 3. Studies with antimicrobial efficacy of Ag-ZnO doped AC and graphene against *E. coli* and *S. aureus*.

Composite	Synthesis method	Concentration/mass	Bacterial type	Inhibition/disinfection	References
Ag-ZnO-AC	Green	34 mg	*S. aureus*	17.33 ± 0.36 mm	This study
			E. coli	14.00 ± 0.37 mm	
Ag/ZnO-AC	Chemical	1000 μg	*S. aureus*	10 mm	[27]
			E. coli	6 mm	
Ag/ZnO/AC	Green	0.12 g	*S. aureus*	8–12 mm	[65]
			E. coli	6–8 mm	
Ag@ZnO-ch NCs	Chemical precipitation	400 μg ml^{-1}	*S. aureus*	14.67 ± 0.58 mm	[66]
			E. coli	9.33 ± 0.58 mm	
ZnAgO/GO	Chemical	100 μl	*S. aureus*	10.73 ± 0.35 mm	[20]
			E. coli	12.44 ± 0.33 mm	

using water hyacinth [54]. Figure 9(b) indicates the presence of Zn and Ag as a result of impregnating Ag-ZnO into the AC matrix.

Microbial assay

The nanocomposite control confirmed no growth of either of the bacterial strains while the bacterial control shows bacterial growth as indicated in the supplementary information S6. This provides a background that, the microbial inhibition has occurred because of the inhibition activity of the nanocomposites synthesized and used in this study. Table 2 demonstrates excellent antimicrobial activities by the Ag-ZnO-AC NCs. The zone of inhibition (ZOI) for Ag-ZnO-AC-650, Ag-ZnO-AC-750, and Ag-ZnO-AC-850 was 13.33 ± 0.21, 13.67 ± 0.33 and 14.00 ± 0.31 mm against *E. coli*, respectively. The inhibition against *S. aureus* for the same nanocomposites was 16.17 ± 0.31, 16.50 ± 0.43 and 17.33 ± 0.36 mm, respectively. These results projected no significant difference since the $p > 0.05$. The results suggest Ag-ZnO NCs are the main antimicrobial agent since the increase of carbonation temperature seems to have little impact. The Ag/ZnO-AC NCs demonstrated stronger antimicrobial activity against *S. aureus* than *E. coli* ($p < 0.05$). However, *S. aureus* bacteria have a thicker outer wall than *E. coli* bacteria, the latter have a peptidoglycan-porin protein membrane composed of lipopolysaccharides. This membrane creates a barrier to prevent antibiotics from penetrating the cell wall making *E. coli* more resistant than *S. aureus* [62, 63].

Although there was no significant difference between the composites prepared with different carbonation temperatures, Ag-ZnO-AC-850 has demonstrated a slightly higher microbial inhibition of 14.00 ± 0.31 and 17.33 ± 0.36 mm for *E. coli* and *S. aureus,* respectively. This might be caused by the sharp edges on the surface of the AC samples which increases the material roughness and fragmentation as observed in the SEM images (figure 6(c)): the sharp edges cause cell walls to rupture and prick [64]. Different masses, 10, 17, and 34 mg were also used to determine the effect of composite mass on microbial inhibition. The increase in mass increased the inhibition of both bacterial strains with a *p*-value less than 0.05 (table 2). The mass increase causes an increase in Ag^{+} and Zn^{2+} ions release which are responsible for microbial inhibition. It contributes to direct nanoparticle attacks forming pits and deformity on the bacterial cells. Similar studies (table 3) reported successful antimicrobial activity on gram-negative (*E. coli*) and gram-positive (*S. aureus*) bacteria. The present study has shown strong antimicrobial activity affirming its promising application as an antimicrobial agent.

The aim of impregnating Ag-ZnO in AC was to reduce the use of the metallic NCs which can be harmful in excess consumption but maintain the excellent antimicrobial activity of the resulting composite. In our previous study, the microbial inhibition of 30 mg Ag-ZnO NCs was 18.17 ± 0.24 mm and 17.19 ± 0.34 mm for *E. coli* and *S. aureus* respectively [40]. In the current study, 34 mg of the Ag-ZnO-AC NCs were used reducing Ag-ZnO by almost 50% since the Ag-ZnO: AC mixing ratio was 1:1. The microbial inhibition of Ag-ZnO-AC NCs was 14.00 ± 0.37 and 17.33 ± 0.36 mm for the *E. coli* and *S. aureus* respectively. The *S. aureus* inhibition was

maintained while that of *E. coli* decreased somehow. Generally, the antimicrobial activity is maintained therefore sustainable use of Ag-ZnO NCs.

Conclusion

Ag-ZnO-AC NCs have been green synthesized successfully using antioxidants extracted from *Launaea cornuta* leaves. The plant extract demonstrated remarkable extraction of antioxidants when extracted by 50% ethanolic solvent $8.598 \pm 0.173\%$ ($44174.19 \pm 93.81\ \mu g\ g^{-1}$) with $P < 0.05$. The XRD results demonstrated successful impregnation of Ag-ZnO into the AC matrix with an average particle size between 40.22 and 50.87 nm. The SEM and TEM images show the formation of sheet-like AC with increased fragmentation on an increase in carbonation temperature. The SEM and TEM images indicate the deposition of spherical crystalline Ag-ZnO into the AC. The antimicrobial activity of the Ag-ZnO-AC NCs has showcased significant results on gram-negative (*E. coli*) and gram-positive (*S. aureus*) bacteria with a maximum inhibition of 14.00 ± 0.37 for *E. coli* and 17.33 ± 0.36 mm for *S. aureus* ($P < 0.05$). These results verify the presence of antioxidants in *Launaea cornuta* and their use in the synthesis of Ag-ZnO-AC NCs with a promising use in microbial inhibition on water treatment.

Acknowledgments

The authors acknowledges: The African Development Bank project and Higher Education Economic Transformation (HEET) project through the Nelson Mandela African Institution of Science and Technology (NM-AIST) for partial funding of the study. The Queen Elizabeth Scholarship-Advanced Scholars program (QES-AS) through the Canadian Queen Elizabeth II Diamond Jubilee Scholarship program funded by Canada's International Development Research Centre [IDRC]. The Erasmus Plus International Credit Mobility Action - student mobility program under the collaboration of the Nelson Mandela African Institution of Science and Technology (NM-AIST) and the University of Milano Bicocca Milan, Italy. Canada Scholarship (SICS) program —Student Exchange Program (SEP) under Global Affairs Canada (GAC) and Carleton University, Canada. Dr Lorenzo Guzetti, Dr Antonia Bruno and Miss. Giulia Ghislen from the Department of Biotechnology and Biosciences—University of Milan Biccoca.

Data availability statement

The data that support the findings of this study will be openly available following an embargo at the following URL/DOI: https://doi.org/10.5061/dryad.gmsbcc2x5. Data will be available from 27 September 2024.

Author contributions

Conceptualization, methodology, formal analysis and investigation, writing—original draft preparation, visualization: E.M.

Conceptualization, methodology, writing—review and editing, supervision: M.R.

Conceptualization, methodology, writing—review and editing, supervision: R.M.

Conceptualization, methodology, writing—review and editing, supervision: O.D.B.

Competing interests

The authors have no competing interests to declare that are relevant to the content of this article.

Conflict of interest

The authors declare that they have no competing interests.

Ethical declarations

Not applicable.

Fundings

Not applicable.

Data availability

Data generated during the study can be accessed through Data Dyad using the link 10.5061/dryad.gmsbcc2 × 5.

ORCID iDs

Elizabeth Makauki https://orcid.org/0009-0002-8104-4293
Mwemezi Rwiza https://orcid.org/0000-0001-5526-444X
Onita D Basu https://orcid.org/0000-0001-5126-0169

References

[1] Zimmer C 2023 *Assessing Point of Use Water Treatment Technologies under Real-Use Conditions: The Field Challenge Test Technique* (University of Victoria)
[2] Ghernaout D, Irki S, Elboughdiri N and Ghernaout B 2023 Solar-driven water treatment: new technologies, challenges, and futures *Green and Sustainable Chemistry* **13** 110–52
[3] Ngai T K K, Shrestha R R, Dangol B, Maharjan M and Murcott S E 2007 Design for sustainable development - household drinking water filter for arsenic and pathogen treatment in Nepal *J. Environ. Sci. Health A Tox Hazard Subst. Environ. Eng.* **42** 1879–88
[4] Arora N K and Mishra I 2022 Sustainable development goal 6: global water security *Environmental Sustainability* 5 271–75
[5] Zamxaka M, Pironcheva G and Nyo M 2004 Microbiological and physico-chemical assessment of the quality of domestic water sources in selected rural communities of the Eastern Cape Province, South Africa *Water SA* **30** 333–40
[6] Li P and Wu J 2019 Drinking water quality and public health *Expo. Health* **11** 73–9
[7] Montagna M T *et al* 2020 Microbiological and chemical assessment of wastewater discharged by infiltration trenches in fractured and karstified limestone (Sca.re.s. project 2019–2020) *Pathogens* **9** 1–20
[8] Foppen J W A 2002 Impact of high-strength wastewater infiltration on groundwater quality and drinking water supply: The case of Sana'a, Yemen *Journal of Hydrology* **263** 198–216
[9] Venis R A and Basu O D 2023 Elution and disinfection of silver and zinc nanoparticles in co-fired ceramic water filters *Sci. Total Environ.* **887** 163317–26
[10] Castro-Muñoz R 2020 The role of new inorganic materials in composite membranes for water disinfection *Membranes (Basel)* **10** 101
[11] Ahmad M and Zhu J 2011 ZnO based advanced functional nanostructures: synthesis, properties and applications *J. Mater. Chem.* **21** 599–614
[12] Madhumitha G, Elango G and Roopan S M 2016 Biotechnological aspects of ZnO nanoparticles: overview on synthesis and its applications *Appl. Microbiol. Biotechnol.* **100** 571–81
[13] Agnihotri S, Bajaj G, Mukherji S and Mukherji S 2015 Arginine-assisted immobilization of silver nanoparticles on ZnO nanorods: an enhanced and reusable antibacterial substrate without human cell cytotoxicity *Nanoscale* **7** 7415–29
[14] Bednář J, Svoboda L, Rybková Z, Dvorský R, Malachová K, Stachurová T, Matýsek D and Foldyna V 2019 Antimicrobial synergistic effect between Ag and Zn in Ag-ZnO.mSiO2 silicate composite with high specific surface area *Nanomaterials* **9** 1265
[15] Jha P K, Pokhum C, Soison P, Techato K A and Chawengkijwanich C 2023 Comparative study of zinc oxide nanocomposites with different noble metals synthesized by biological method for photocatalytic disinfection of *Escherichia coli* present in hospital wastewater *Water Sci. Technol.* **88** 1564–77
[16] Ma S, Zhan S, Xia Y, Wang P, Hou Q and Zhou Q 2019 Enhanced photocatalytic bactericidal performance and mechanism with novel Ag/ZnO/g-C_3N_4 composite under visible light *Catal. Today* **330** 179–88
[17] Venkatraman G, Mohan P S, Abdul-Rahman P S, Sonsudin F, Muttiah B, Hirad A H, Alarfaj A A and Wang S 2024 Morinda citrifolia leaf assisted synthesis of ZnO decorated Ag bio-nanocomposites for *in-vitro* cytotoxicity, antimicrobial and anticancer applications *Bioprocess. Biosyst. Eng.* **47** 1213–26
[18] Scaria S S and Joseph K S 2024 Exploring the photocatalytic and cytotoxic potential of quassia indica-derived bimetallic silver-zinc oxide nanocomposites *Waste Biomass Valorization* **2024** 1–15
[19] Asamoah R B, Yaya A, Nbelayim P, Annan E and Onwona-Agyeman B 2020 Development and characterization of clay-nanocomposites for water purification *Materials* **13** 3793–821
[20] Khan A, Kamal T, Saad M, Ameen F A, Bhat S, Ahamad Khan M and Rahman F 2023 Synthesis and antibacterial activity of nanoenhanced conjugate of Ag-doped ZnO nanorods with graphene oxide *Spectrochim. Acta A Mol. Biomol. Spectrosc.* **290** 122296–305
[21] Panchal P, Paul D R, Sharma A, Choudhary P, Meena P and Nehra S P 2020 Biogenic mediated Ag/ZnO nanocomposites for photocatalytic and antibacterial activities towards disinfection of water *J. Colloid Interface Sci.* **563** 370–80
[22] Alherek M and Basu O D 2023 Impact of low levels of silver, zinc and copper nanoparticles on bacterial removal and potential synergy in water treatment applications *J. Chem. Technol. Biotechnol.* **98** 1137–46
[23] Hassan H S, Deyaa A, Salama E and Elkady M F 2022 Assessment of antimicrobial, cytotoxicity, and antiviral impact of a green zinc oxide/activated carbon nanocomposite *Scientific reports* **12** 8774
[24] Kumar-Krishnan S, Prokhorov E, Hernández-Iturriaga M, Mota-Morales J D, Vázquez-Lepe M, Kovalenko Y, Sanchez I C and Luna-Bárcenas G 2015 Chitosan/silver nanocomposites: synergistic antibacterial action of silver nanoparticles and silver ions *Eur. Polym. J.* **67** 242–51
[25] Ai T *et al* 2021 Microstructure and properties of Ag-doped ZnO grown hydrothermally on a graphene-coated polyethylene terephthalate bilayer flexible substrate *Front. Chem.* **9** 661127–33
[26] Belachew N, Kahsay M H, Tadesse A and Basavaiah K 2020 Green synthesis of reduced graphene oxide grafted Ag/ZnO for photocatalytic abatement of methylene blue and antibacterial activities *J. Environ. Chem. Eng.* **8** 104106

[27] Kumar T P, Triveni R M, Sangeetha P, Sakthivel P, Revathi S K, Kumar A S and Suban K S 2015 Highly Efficient Performance of Activated Carbon Impregnated with Ag, ZnO and Ag/ZnO nanoparticles as Antimicrobial Materials *RSC Advances* **5** 108034–43 RSC Adv. American Institute of Chemical Engineers
[28] Moradi M, Haghighi M and Allahyari S 2017 Precipitation dispersion of Ag–ZnO nanocatalyst over functionalized multiwall carbon nanotube used in degradation of acid orange from wastewater *Process Safety and Environmental Protection* **107** 414–27
[29] Das S, Ranjana N, Misra A J, Suar M, Mishra A, Tamhankar A J, Lundborg C S and Tripathy S K 2017 Disinfection of the waterborne pathogens *Escherichia coli* and *Staphylococcus aureus* by solar photocatalysis using sonochemically synthesized reusable Ag@ZnO core–shell nanoparticles *Int. J. Environ. Res. Public Health* **14** 747
[30] Shabaani M, Rahaiee S, Zare M and Jafari S M 2020 Green synthesis of ZnO nanoparticles using loquat seed extract; biological functions and photocatalytic degradation properties *LWT* **134** 110133
[31] Lichtfouse E, Schwarzbauer J and Robert D 2005 (Environmental chemist)*Environmental chemistry : Green Chemistry and Pollutants in Ecosystems* (Springer)
[32] Kharissova O V, Dias H V R, Kharisov B I, Pérez B O and Pérez V M J 2013 The greener synthesis of nanoparticles *Trends Biotechnol.* **31** 240–8
[33] Priya N, Kaur K and Sidhu A K 2021 Green synthesis: an eco-friendly route for the synthesis of iron oxide nanoparticles *Frontiers in Nanotechnology* **3** 655062–77
[34] Naseer M, Aslam U, Khalid B and Chen B 2020 Green route to synthesize zinc oxide nanoparticles using leaf extracts of cassia fistula and melia azadarach and their antibacterial potential *Sci. Rep.* **10** 9055–64
[35] Kalaba M H, Moghannem S A, El-Hawary A S, Radwan A A, Sharaf M H and Shaban A S 2021 Green synthesized ZnO nanoparticles mediated by Streptomyces plicatus: characterizations, antimicrobial and nematicidal activities and cytogenetic effects *Plants* **10** 1760–85
[36] Guzmán M G, Dille J and Godet S 2009 Synthesis of silver nanoparticles by chemical reduction method and their antibacterial activity *International Journal of Chemical and Biomolecular Engineering* **2** 104–7
[37] Aritonang H F, Koleangan H and Wuntu A D 2019 Synthesis of silver nanoparticles using aqueous extract of medicinal plants' (Impatiens balsamina and Lantana camara) fresh leaves and analysis of antimicrobial activity *Int. J. Microbiol.* **10** 1–8
[38] Pirtarighat S, Ghannadnia M and Baghshahi S 2019 Green synthesis of silver nanoparticles using the plant extract of salvia spinosa grown *in vitro* and their antibacterial activity assessment *J. Nanostructure Chem.* **9** 1–9
[39] Yong J, Beom S Æ and Kim S 2009 Rapid biological synthesis of silver nanoparticles using plant leaf extracts *Bioprocess. Biosyst. Eng.* **32** 79–84
[40] Makauki E, Mtavangu S G, Basu O D, Rwiza M and Machunda R 2023 Facile biosynthesis of Ag–ZnO nanocomposites using Launaea cornuta leaf extract and their antimicrobial activity *Discover Nano* **18** 142
[41] Bouguerra A, Hadjadj M, Dekmouche M, Rahmani Z and Dendougui H 2019 Determination of phenolic content and antioxidant capacity of launaea resedifolia from algerian sahara *J. Appl. Biol. Biotechnol.* **7** 63–9
[42] Guzzetti L, Panzeri D, Ulaszewska M, Sacco G, Forcella M, Fusi P, Tommasi N, Fiorini A, Campone L and Labra M 2021 Assessment of dietary bioactive phenolic compounds and agricultural sustainability of an african leafy vegetable corchorus olitorius L *Front Nutr.* **8** 667812–21
[43] Makauki E, Cecil K K and Talam E K 2017 Hydrogen sulfide and ammonia removal from biogas using water hyacinth-derived carbon nanomaterials *Afr. J. Environ. Sci. Tech.* **11** 375–83
[44] Khalil M M H, Ismail E H, El-Baghdady K Z and Mohamed D 2014 Green synthesis of silver nanoparticles using olive leaf extract and its antibacterial activity *Arabian J. Chem.* **7** 1131–9
[45] Gertenbach D D 2016 Solid-liquid extraction technologies for manufacturing nutraceuticals *Functional Foods: Biochemical and Processing Aspects* ed J Shi, G Mazza and M L Maguer (Boca Raton: CRC Press LLC) 11, 331–66
[46] Suwarno A C, Yulizar Y, Apriandanu D O B and Surya R M 2022 Biosynthesis of Dy2O3 nanoparticles using piper retrofractum vahl extract: optical, structural, morphological, and photocatalytic properties *J. Mol. Struct.* **1264** 133123–32
[47] Wang Y Y, Li J Q, Liu H G and Wang Y Z 2019 Attenuated total reflection-Fourier transform infrared spectroscopy (ATR-FTIR) combined with chemometrics methods for the classification of Lingzhi species *Molecules* **24** 2210
[48] Ahmad S, Nawaz F, Naheed S, Ahmad Z and Mehmmod T 2019 Phytochemical screening by FTIR spectroscopic analysis of leaf extracts of monotheca buxifolia *UW Journal of Science and Technology* **3** 15–22 https://uwjst.org.pk/index.php/uwjst/article/view/19
[49] Hemmati S, Rashtiani A, Zangeneh M M, Mohammadi P, Zangeneh A and Veisi H 2019 Green synthesis and characterization of silver nanoparticles using fritillaria flower extract and their antibacterial activity against some human pathogens *Polyhedron* **158** 8–14
[50] Yulizar Y, Gunlazuardi J, Apriandanu D O B and Syahfitri T W W 2020 CuO-modified CoTiO3 via catharanthus roseus extract: a novel nanocomposite with high photocatalytic activity *Mater. Lett.* **277** 128349–53
[51] Elviera, Yulizar Y, Apriandanu D O B and Marcony Surya R 2022 Fabrication of novel SnWO4/ZnO using muntingia calabura l. leaf extract with enhanced photocatalytic methylene blue degradation under visible light irradiation *Ceram. Int.* **48** 3564–77
[52] Morales S L, Baas-López J M, Barbosa R, Pacheco D and Escobar B 2021 Activated carbon from water hyacinth as electrocatalyst for oxygen reduction reaction in an alkaline fuel cell *Int. J. Hydrogen Energy* **46** 25995–6004
[53] Masakul P, Nilmoung S, Sonsupap S and Laorach L 2023 The electrochemical properties of water hyacinth-derived activated carbon *Journal of Metals, Materials and Minerals* **33** 2–7
[54] Masto R E, Kumar S, Rout T K, Sarkar P, George J and Ram L C 2013 Biochar from water hyacinth (Eichornia crassipes) and its impact on soil biological activity *Catena (Amst)* **111** 64–71
[55] Tomczyk A, Sokołowska Z and Boguta P 2020 Biomass type effect on biochar surface characteristic and adsorption capacity relative to silver and copper *Fuel* **278** 118168–77
[56] Liu Y, Zhao X, Li J, Ma D and Han R 2012 Characterization of bio-char from pyrolysis of wheat straw and its evaluation on methylene blue adsorption *Desalination Water Treat* **46** 115–23
[57] Choudhary M K, Kataria J, Bhardwaj V K and Sharma S 2019 Green biomimetic preparation of efficient Ag-ZnO heterojunctions with excellent photocatalytic performance under solar light irradiation: a novel biogenic-deposition-precipitation approach *Nanoscale Adv* **1** 1035–44
[58] Ashraf H, Anjum T, Riaz S and Naseem S 2020 Microwave-assisted green synthesis and characterization of silver nanoparticles using melia azedarach for the management of fusarium wilt in tomato *Front. Microbiol.* **11** 238–59
[59] Mehta B K, Chhajlani M and Shrivastava B D 2017 Green synthesis of silver nanoparticles and their characterization by XRD *J. Phys. Conf. Ser.* (Institute of Physics Publishing) 012050–4

[60] Vo N T T, Do M Q, Pham V and Van 2023 Green chemistry synthesis and *Escherichia coli* antibacterial activity of silver and zinc oxide nanoparticles *J. Aust. Ceram. Soc.* **59** 1205–12
[61] Suman S, Panwar D S and Gautam S 2017 Surface morphology properties of biochars obtained from different biomass waste *Energy Sources Part* A **39** 1007–12
[62] Al-Gaashani R, Pasha M, Jabbar K A, Shetty A R, Baqiah H, Mansour S, Kochkodan V and Lawler J 2023 Antimicrobial activity of ZnO-Ag-MWCNTs nanocomposites prepared by a simple impregnation–calcination method *Sci. Rep.* **13** 21418–34
[63] Bala N, Saha S, Chakraborty M, Maiti M, Das S, Basu R and Nandy P 2015 Green synthesis of zinc oxide nanoparticles using Hibiscus subdariffa leaf extract: effect of temperature on synthesis, anti-bacterial activity and anti-diabetic activity *RSC Adv.* **5** 4993–5003
[64] Liu S, Wei L, Hao L, Fang N, Chang M W, Xu R, Yang Y and Chen Y 2009 Sharper and faster 'nano darts' kill more bacteria: a study of antibacterial activity of individually dispersed pristine single-walled carbon nanotube *ACS Nano* **3** 3891–902
[65] Taha A, Aissa M, Ben and Da'na E 2020 Green synthesis of an activated carbon-supported Ag and ZnO nanocomposite for photocatalytic degradation and its antibacterial activities *Molecules* **25** 1586–604
[66] Raj Kumar S and Gopinath P 2017 *In situ* synthesis of chitosan coated silver-zinc oxide nanocomposites and its enhanced antibacterial properties *J. Nanosci. Nanotechnol.* **17** 8797–805